International Journal of Biological Macromolecules 332 (2025) 148655

Contents lists available at ScienceDirect

International Journal of Biological Macromolecules

journal homepage: www.elsevier.com/locate/ijbiomac

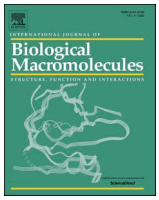

One-pot synthesis of silver-based chitosan macromolecular hydrogels and its antimicrobial activity

S. Pouri [a], I. Fraile-Gutiérrez [b], R. Gil-Gonzalo [a], N. Acosta [a,c], F. Navarro-García [d], I. Aranaz [a,c,*]

[a] Instituto Pluridisciplinar, Universidad Complutense de Madrid, Paseo de Juan XXIII, n°1, Madrid, 28040, Spain
[b] Laboratory of Organ Printing, University of Bayreuth, 95447, Bayreuth, Germany
[c] Departamento de Química en Ciencias Farmacéuticas, Facultad de Farmacia, Universidad Complutense de Madrid, Plaza Ramón y Cajal S/N, Madrid, 28040, Spain
[d] Departamento de Microbiología y Parasitología, Facultad de Farmacia, Universidad Complutense de Madrid, Plaza Ramón y Cajal S/N, Madrid, 28040, Spain

ARTICLE INFO

Keywords:
Silver nanoparticles
Chitosan
Antimicrobial activity

Chemical compounds studied in this article:
Chitosan (PubMed CID: 71853)
Silver nitrate (PubMed CID: 24470)
1,3 propane sultone (PubMed CID: 14264)
Potassium nitrite (PubMed CID: 24449)

ABSTRACT

This study focused on the description of a new methodology for preparing AgNP-loaded chitosan-based hydrogels *via* a one-pot procedure through the thermal decomposition of urea. This new methodology enhanced the controlled production of AgNPs by increasing the viscosities of the polymeric solutions and controlling the pH basification, thereby favoring nanoparticle nucleation over aggregation, resulting in the production of AgNPs with sizes lower than 20 nm. Four types of chitosan samples, including two native samples with different molecular weights and their sulfated salts, were studied.

AgNPs synthesis was characterized following Surface Plasmon Resonance and by TEM microscopy, while simultaneous hydrogel formation was followed by viscometry. The synthesized AgNPs were pseudospherical in shape with a narrower distribution and smaller size for those samples produced with chitosan salts. The AgNPs-chitosan samples exhibited moderate antioxidant and antimicrobial activities against *E. coli* ATCC 25923 and *S. aureus* ATCC 25922 with inhibition zones of around 13 mm in the best formulations. These properties indicate the potential of these materials as wound-healing agents.

1. Introduction

Metallic-based nanoparticles are of great interest in various fields, including catalysis, energy, water treatment, biomedicine, the food industry, and agriculture, among others [1–5]. In particular, silver nanoparticles (AgNPs) are widely used in wound healing not only due to their antimicrobial activity but also due to their antioxidant and anti-inflammatory activities [6,7].

The production of nanoparticles can be carried out using an up-down or bottom-up approach. In the first approach, the bulk material is broken down into small pieces using various techniques, such as ball milling, thermal evaporation, and laser ablation [8–10]. In the second approach, nanoparticles are formed atom by atom to assemble into clusters that finally produce the nanoparticles [11]. Metallic nanoparticles tend to agglomerate due to their high active surface area. Different types of molecules, such as surfactants, polymers, biomacromolecules (including proteins and DNA), or dendrimers, are used to stabilize and control the size and shape of AgNPs [12–18].

As previously reported, one strategy to control the properties of AgNPs is to produce them within hydrogels [19,20]. In these works, hydrogels were produced in the first step, and subsequently, they were introduced into a solution containing silver salts, allowing the silver ions to be absorbed by the polymer network or just entrapped in the free space existing between the gel networks. The driving process for silver loading was the ion exchange between Ag^+ and H^+ groups in the polymer network, so this methodology cannot be applied to neutral networks. Silver salts have been loaded into colloidal polymeric particles, producing AgNPs-loaded micro-hydrogels, which are micron-sized cross-linked polymeric networks, that have also been developed to be used in neutral networks [21]. In all these approaches, once the silver salt is incorporated into the polymer network, a second step is necessary to produce the silver nanoparticles by Ag^+ reduction with $NaBH_4$.

Chitosan is a copolymer of *N*-acetylglucosamine and glucosamine with exceptional properties in biomedicine such as anti-inflammatory, antimicrobial or antioxidant activities [22]. Moreover, chitosan has been an accepted excipient in the pharmacopoeia since 2011 [23], thereby increasing the interest in this polymer in the biomedical and pharmaceutical fields. Chitosan has been successfully used to stabilize

* Corresponding author at: Instituto Pluridisciplinar, Universidad Complutense de Madrid, Paseo de Juan XXIII, n°1, Madrid, 28040, Spain.
E-mail address: iaranaz@ucm.es (I. Aranaz).

https://doi.org/10.1016/j.ijbiomac.2025.148655
Received 25 April 2025; Received in revised form 5 October 2025; Accepted 28 October 2025
Available online 29 October 2025

silver nanoparticles in combination with chemical reductants [24,25]. However, although it has been reported that it can also be used as a reductant and stabilizer of silver ions to produce silver nanoparticles sometimes poor control in the size and distribution of the AgNPs is observed and therefore, in some cases, dark brown and grey solutions are produced instead of the typical yellowish solution observed in small colloidal AgNPs solutions due to their Surface Plasmon Resonance (SPR) [26–29]. This can be explained as chitosan is not a unique molecule but a large family of polymers with different physicochemical properties that exert a strong influence on chitosan properties in various applications. The variability in the behavior of chitosan samples regarding their ability to reduce and stabilize AgNPs, underlying the need for optimizing reaction parameters (*e.g.*, pH, chitosan concentration, and precursor ratios), introducing chemical modifications (i.e., production of salts such as chitosan propane sulfate) or introducing an environmental control as previously mentioned for better control over AgNPs size and dispersion during the assisted-chitosan-synthesis. Chitosan needs to be solubilized in acidic media conditions, and in previous studies, we have observed that this acidic pH appears to negatively affect its ability to control the properties of AgNPs. Our results have shown that better control in the synthesis of AgNPs is achieved when soluble-in-water chitosan salts (sulfated chitosan) or soluble-in-water low-molecular-weight chitosan are produced from those samples that are unable to form and stabilize AgNPs [26,27]. Cao et al. have also demonstrated the good performance of soluble-in-water chitosan derivatives to produce AgNPs [30]. Chitosan can form physical hydrogels easily by neutralizing the acidic environment under proper physicochemical conditions, which may create an appropriate environment for AgNPs growth.

The neutralization of the polymeric solution results in a modification of the balance between hydrophobic and hydrophilic interactions in the polymer chains, due to the reduction in the apparent positive charge resulting from glucosamine deprotonation [31,32]. Such a procedure occurs in the presence of a base such as NaOH, KOH, or ammonium. The thermal or urease-mediated decomposition of urea also renders the formation of chitosan hydrogels [33,34]. Interestingly, thermal urea decomposition to produce ammonia can be carried out at around 90 °C, which falls within the temperature range for the thermal production and stabilization of AgNPs in chitosan [33,35] Furthermore, urea is biocompatible, and the presence of urea in formulations can increase skin penetration and optimize the action of topical drugs [36].

Several studies on the morphology of chitosan physical hydrogels have been conducted. Sereni et al. described the morphology of hydrogels neutralized with NaOH as a gradient from the surface to the bulk, with mainly two structural hydrogel transition zones separating three types of hydrogels [37]. Zhengbo et al. showed that physical hydrogels produced by dissolving chitosan in urea/NaOH solutions at low temperature and subsequently heated and soaked to remove the solvent generate a primary network produced during thermal gelation due to poor chitosan solubility in such conditions, followed by the deposition and crystallization of chitosan during solvent displacement [38]. Hydrogels produced by thermal treatment in the presence of urea are expected to form homogeneous hydrogels, as urea is homogeneously dissolved in the chitosan solution. Therefore, the modification of the pH occurs in a controlled manner inside the polymer solution.

In this paper, we hypothesize that it is possible to produce controlled AgNPs within a chitosan-based hydrogel through a one-step procedure involving the thermal decomposition of urea at 90 °C. This new methodology avoids the more tedious previously discussed strategies for producing silver nanoparticles within hydrogels in multi-step procedures. Additionally, by thermally decomposing urea, we can not only avoid chemicals, such as monomers or reducing agents, that may compromise the biocompatibility of the hydrogel for subsequent biomedical applications but also improve these qualities, as urea is biocompatible and several positive effects on wound healing have been described for this molecule [36].

For this purpose, four different polymers were evaluated i) two chitosan samples with different molecular weights that have demonstrated no ability to stabilize silver nanoparticles in acidic solution, and ii) two chitosan salts derived from the aforementioned chitosan samples that have proven their ability to reduce and stabilize AgNPs [26].

2. Materials and methods

2.1. Materials

Chitosan from crustacean origin (CHT1) was kindly donated by InFiQuS S.L. (Madrid, Spain). 1,3-Propanesultone (purity ≥99.0 %), KNO_2 (purity ≥96 %), 2,2-difenil-1-picrilhidrazil (DPPH), 2, 4, 6-tripyridyl-*s*-triazine (TPTZ) (purity ≥98 %), ammonium acetate (for analysis, purity ≥99.0 %), urea (ACS reagent grade), $AgNO_3$ (purity ≥99.0 %), *N*-acetyl glucosamine (Pharmaceutical Secondary Standard), and Trolox were purchased from Sigma-Aldrich (St. Louis, MO, USA). Acetic acid (pharma grade), methanol (for analysis, ACS grade), and HCL 37 % were purchased from Panreac (Madrid, Spain). Mueller-Hinton Agar was purchased from Labbox (Barcelona, Spain).

2.2. Chitosan modification

The parent chitosan sample (CHT1) was chemically depolymerized as previously described using KNO_2/HCl to produce the low-molecular-weight chitosan sample, denoted as CHT2 [39]. To produce sulfated chitosan salts, both CHT1 and CHT2 chitosan samples were dissolved at 1 % *w/v* overnight in 0.2 M acetic acid and subsequently heated at 60 °C in the presence of 1,3 propane sultone (chitosan amino group: propane sultone molar ratio 1:1) for 6 h under magnetic stirring. The final polymeric products of the reaction (CHT1S and CHT2S, respectively) were purified by dialysis and recovered by lyophilization (Telstar Lyo-Quest 55) as previously described [40].

2.3. Polymer characterization

The UV-first derivative spectroscopy method was employed to determine the degree of chitosan acetylation [41]. Briefly, chitosan samples were dissolved at a concentration of 1 mg/mL in 0.1 M acetic acid overnight. The spectra of the 10 times diluted in water samples were recorded between 190 and 240 nm using a UV–VIS spectrophotometer (Specord 205 Analytik Jena). Standard solutions of *N*-acetylglucosamine were prepared in acetic acid 0.01 M at a concentration ranging from 0 to 0.04 mg/mL.

The calibration curve was created by plotting the first derivative of UV spectra values at 202 nm against the *N*-acetylglucosamine concentration.

The acetylation degree was calculated according to Eq. (1)

$$\mathrm{DA} = \frac{[NAG]}{[chitosan]} * 100 \quad (1)$$

where [NAG] is the concentration of *N*-acetylglucosamine calculated from the calibration curve.

Gel Permeation Chromatography (GPC) was used to determine the molecular weight of chitosan. Samples were dissolved (1 mg/mL) in the mobile phase (Ammonium acetate buffer, 0.15 M, pH 4.5) and filtered through a 0.45 μm syringe filter before injection. GPC was performed with a Waters 625 LC System Pump connected to a refractive index detector. A size-exclusion chromatography column (Ultrahydrogel TM1000, 7.8 × 300 mm, Waters) at a flow rate of 0.6 mL/min at 35 °C was used. A set of narrow dextran standards was used to create the calibration curve for determining Mw, Mn, and PDI (Dextran Standard Kit, Waters, USA).

2.4. One-pot silver nanoparticle synthesis and polymer gelation

A solution of silver nitrate ($AgNO_3$) was prepared by dissolving the salt in water at concentrations of 5 mM, 10 mM, 20 mM, and 40 mM. For each concentration, 200 μL of the $AgNO_3$ solution was mixed with 1 mL of a polymer solution (polymer concentration 1 % *w/v*, in acetic acid 0.1 M, stirred overnight). Additionally, 200 μL of a 2 M urea solution in water was added to this mixture. The mixtures were heated at 90 °C (themoblock, Selecta, Spain), and gel formation was determined by the inversion tube method and viscometry. Each sample was measured in triplicate. For the gelation studies, the gelling times of the different chitosan and chitosan salt solutions in the presence of silver and urea were determined at 90 °C using a programmable viscometer (Fungilab Premium Series, Barcelona, Spain) with a small sample adaptor and spindle TR8 at 100 rpm. A total of 7.0 mL of a 1 % (*w/v*) chitosan solution, or chitosan salt, was combined with 1.750 mL of 2 M urea and 1.4 mL of 40 mM $AgNO_3$ for the preparation of hydrogels containing AgNPs. Immediately afterward, 7.1 mL of this mixture was poured into a preheated sample container. To prevent evaporation during the tests, mineral oil was used to cover the surface of the chitosan solutions. The effect of mineral oil on the measurements was shown to be negligible. Gelling time was noted as the time at which the mixture's viscosity begins to increase sharply to reach the maximum. Control samples without silver were also studied. Each sample was measured in duplicate.

2.5. AgNPs characterization

The formation of AgNPs was followed in a NanoDrop One (Thermo Scientific). For this purpose, 20 μl of the mixture was taken until the solution was too viscous to be withdrawn, and the absorbance was measured between 300 nm and 700 nm. AgNPs morphology and size were evaluated under Transmission Electronic Microscopy (JEM 1200 HT, Tokyo, Japan) while the crystalline structure was elucidated by Selected Area Electron Diffraction (SAED) at ICTS National Centre of Electronic Microscopy (Complutense University). For TEM analysis, AgNPs-loaded hydrogels were sonicated in acetone for 5 min, and a drop (around 10 μl) of the acetone solution was added to the grid. TEM images were analyzed with ImageJ software (National Institutes of Health, USA), and histograms were generated with Origin Pro 2021 software (OriginLab Corporation, Northampton, MA, USA).

2.6. Antioxidant activity

Immediately after hydrogel formation, the samples were lyophilized and kept at room temperature in the dark until the antioxidant activity assay. Lyophilized hydrogels without silver were also prepared as a control. Each sample was analyzed in triplicate.

2.6.1. Free radical scavenging activity (DPPH assay)

The lyophilized hydrogels were tested for their antioxidant activity by DPPH method [42]. The DPPH assay is based on the reduction of 1, 1-diphenyl-2-picrylhydrazyl, changing the color from red to yellow. 1 mg of each sample was added to 1 mL of methanolic solution containing DPPH radicals (0.1 mM). The antioxidant activity of the control lyophilized hydrogels was also determined at 1, 5, and 10 mg/mL. Once samples were put in contact with the DPPH solution, the mixture was vortexed, and after 60 min in the dark, the absorbance was determined at 517 nm (Specord 205 Analytik Jena). A sample-free DPPH solution prepared following the same procedure was used as a control. Free radical scavenging activity was expressed as the percentage of inhibition, calculated according to Eq. (2).

$$Inhibition\% = \frac{(Abs\ control - Abs\ sample)}{Abs\ control} * 100 \quad (2)$$

where Abs control is the control absorbance of the sample-free DPPH solution; Abs sample is the sample absorbance of DPPH radical + sample (with or without AgNPs).

2.6.2. Ferric reducing antioxidant power (FRAP) assay

FRAP assay was performed as previously described [43]. This method is based on the ability of antioxidants to reduce Fe^{+3} to Fe^{+2} in the presence of TPTZ (2, 4, 6-tripyridyl-*s*-triazine), forming an intense blue Fe^{+2} – TPTZ complex. FRAP solution (0.9 mL) was added to 1 mg of lyophilized samples or polymer solutions (1, 5, and 10 mg/mL) and incubated at 37 °C for 30 min. The absorbance was measured at 595 nm (Specord 205 Analytik Jena) and compared to a Trolox standard curve. The FRAP values were expressed as micro equivalents of Trolox.

2.7. Antimicrobial activity

Bacterial inoculum was prepared according to the guidelines selected by the Clinical and Laboratory Standards Institute (CLSI) using the Kirby-Bauer disk diffusion method [44]. Briefly, a 0.5 McFarland dilution of an overnight culture of *Escherichia coli* ATCC 25922 or *Staphylococcus aureus* ATCC 25923 was streaked onto Mueller-Hinton Agar (MHA) plates using a swab to produce a lawn of the selected microorganisms. After that, blank antibiotic disks were dipped in the different concentrations of AgNPs-polymer (5, 10, 20, and 40 mM, as described in Section 2.4) and sterilized under UV light. After sterilization, the embedded disks were placed onto the inoculated MHA plates. Control experiments using disks embedded in different chitosans without silver nanoparticles were performed for comparison. After overnight incubation at 37 °C, the antibacterial activity was assessed by measuring the zones of inhibition around each hydrogel. The diameter of the clear area (zone where bacterial growth was inhibited) was measured in millimeters (mm) using a standard ruler. Measurements were taken from edge to edge across the center of the zone. All experiments were performed in triplicate.

2.8. Data analysis

Assay data are expressed as the mean value ± standard deviation. Histograms from TEM images were generated with Origin Pro 2021 software (OriginLab Corporation, Northampton, MA, USA). At least 100 representative nanoparticles per sample were analyzed to produce the histograms.

3. Results and discussion

It is well known that chitosan physical hydrogels can be easily produced by modifying the pH of the polymer solution in a controlled manner [45]. Chitosan solubility in an acidic solution is attributed to the protonation of the primary amino groups in the glucosamine moieties, which induces electrostatic repulsion between the polymer chains. Hydrophobic interactions are encouraged, and the gel-like precipitation occurs when $-NH_2$ is deprotonated at pH above its pKa (6.3–7). Different chemicals, such as NaOH, KOH, ammonium vapors, or urea, have been proposed to produce physically crosslinked chitosan hydrogels [37,38,46]. Urea decomposition can be achieved by thermal or enzymatic procedures [33,47]. In an initial series of experiments, we investigated the time required to produce chitosan hydrogels through thermal urea decomposition at 90 °C using two chitosan samples with different molecular weights (Samples CHT1 and CHT2) and examined how these samples behave once the sulfated salts are produced (Samples CHT1S and CHT2S, respectively). The main physicochemical properties of the polymers, along with the time required for each polymer solution to form a gel using the inversion tube method, are presented in Table 1. The CHT1 sample produced hydrogels in a shorter time than the CHT2 sample. This effect was merely due to the difference in the molecular weight, since the initial pH and acetylation degree of both solutions were quite similar, as shown in Table 1. This can be explained by

Table 1
Main characteristics of chitosan and sulfated chitosan salts and time to gel by inversion tube methodology.

Sample	Acetylation degree, %[a]	Mw, kDa	Mn, kDa	PDI	Solution pH	Gelling time, min[a]
CHT1	12.2 ± 0.5	1185	37	31	4.37	240 ± 20
CHT2	12.2 ± 0.4	162	23	7	4.39	340 ± 20
CHT1S	11.4 ± 0.4	779	36	21	3.74	300 ± 30
CHT2S	11.4 ± 0.4	93	22	4	3.66	-[b]

[a] Each experiment was repeated three times.
[b] Small gel fragments were formed, and tube inversion is not a proper technique to determine gelation time.

considering that longer polymer chains generate more viscous solutions and can form more entanglements and junctions, thereby facilitating faster network formation [48,49].

Comparing CHT1 sample with its salt (CHT1S), the salt had a longer gel formation time, although the molecular weight of sample CHT1S is lower. When analyzing both polymers, no relevant differences in the degree of acetylation of the samples were observed, and a slight reduction in the molecular weight (approximately 1.5-fold) was noted. We determined the initial pH of the solutions, and in all cases, the chitosan solutions exhibited a higher pH than their salts (Table 1). Therefore, the different behavior can be mainly attributed to the solution pH. The lower the initial pH, the larger the number of amine groups to be deprotonated, and more base is needed to increase the solution pH, since the polymers were dissolved in an excess of acid.

When the chitosan salt from low molecular weight was tested (CHT2S), accurately determining the gelling point was difficult, as it tended to form multiple small gel fragments instead of a single piece of hydrogel; therefore, this methodology was not applied.

When silver nitrate was added to the polymeric solution (chitosan or chitosan salt) and heated in the presence of urea, the gels were also formed. Adding silver to the solutions did not alter the time required to produce the gels except at a high silver concentration (40 mM), as shown in Table 2. This effect was observed mainly in the samples with the highest molecular weight (CHT1 and CHT1S). Previous studies have demonstrated the ability of chitosan and silver nitrate to produce continuous hydrogels from chitosan solutions [50]. The production of such hydrogels depends on the concentration of both components (chitosan and silver nitrate). In this work, we used a polymer concentration of 10 mg/mL, which is high enough to exceed the critical concentration (c^*) of our chitosan samples. Since the concentration of the solutions was higher than c^*, the formation of a continuous hydrogel in the presence of silver nitrate is expected [50]. Therefore, two crosslinking phenomena occurred in our hydrogels (Scheme 1). A soft crosslinked network was generated as soon as chitosan and silver nitrate were put in contact. In this first step, the random chitosan coils act as a nanoreactor, where Ag^+ ions are coordinated with functional chitosan groups, cross-linking polymer chains within the coil volume [35]. The gelation process continued with the deprotonation of chitosan, resulting from urea decomposition, which rendered a more stable hydrogel due to the new hydrogen bonds between polymer chains. The reason why the jellification time is reduced at 40 mM may be that, as more $AgNO_3$ is included in the chitosan solution, it is more likely that the formation of additional cross-links between chitosan chains and silver occurs [50]. Moreover, it has been reported that the mere presence of silver nanoparticles could increase the gel strength and crosslinking density of gel made of acrylic acid (AA), poly(ethylene glycol) methyl ether acrylate (PEGMEA), also supporting our results [51].

Table 2
Gelation time of chitosan-urea solutions at different $AgNO_3$ concentrations by inversion tube.

Sample	$AgNO_3$ 5 mM, min[a]	$AgNO_3$ 10 mM, min	$AgNO_3$ 20 mM, min	$AgNO_3$ 40 mM, min[a]
CHT1	240 ± 20	240 ± 20	240 ± 20	120 ± 20
CHT2	340 ± 20	340 ± 20	320 ± 20	300 ± 20
CHT1S	330 ± 30	330 ± 30	300 ± 30	180 ± 30
CHT2S	-[b]	-[b]	-[b]	-[b]

[a] Each experiment was repeated three times.
[b] Small gel fragments were formed, and tube inversion is not a proper technique to determine gelation time.

In order to study the gelling process in more detail, we studied the variation of the viscosity during gel formation. Due to the equipment's characteristics, we were also able to clearly observe changes in the color of the silver-containing solutions and the turbidity prior to gelation. In all cases, the sharp increase in viscosity, due to gel formation, was observed at lower times in the presence of silver (40 mM) than in the control samples without silver, in good agreement with the data from the inversion tube analysis (Table 3, Fig. 1S).

During the gelation assay, chitosan solutions with silver turned dark brown, while sulfated samples were yellowish at initial times and turned reddish as the experiment proceeded. To determine whether the change in solution color was due to the formation of metallic silver nanoparticles, we monitored the AgNPs surface plasmon resonance (SPR) using UV–Vis spectroscopy. Measurements were taken at different times while the media was manageable. Figs. 1 and 2 illustrate the formation of silver nanoparticles over time at varying silver concentrations during the preparation of chitosan hydrogels. In sample CHT1, data was only collected at 60 min, as the solution became too viscous to be withdrawn from the media. At low silver concentration (5 mM), no clear band was observed, while bands around 400–450 nm appeared at the highest concentrations. In the sample CHT2, no band was observed at a low silver concentration (5 mM–10 mM), while a clear band was observed at 20 and 40 mM. It is remarkable that in a previous paper, we demonstrated that samples CHT1 and CHT2 were unable to stabilize silver nanoparticles thermally produced in acidic media, resulting in grey solutions without SPR [26]. In this work, the production of AgNPs occurs simultaneously with the jellification process, thereby hindering the movement of the AgNPs and preventing aggregation. Additionally, the acidic medium appears to harm the stability of AgNPs, as our results have shown that producing silver nanoparticles in water using water-soluble chitosan salts, thereby avoiding the use of acetic acid, yields a more symmetric SPR band [26]. Other authors have also reported the production of silver nanoparticles using chitosan in suspension in basic media, rather than dissolving it in acidic media [52]. Therefore, we hypothesized that both the increase in viscosity due to jellification and the increase in pH due to urea decomposition positively affect the stabilization of AgNPs in chitosan solutions, allowing us to produce AgNPs rather than large aggregates, as observed in our previous work.

When the chitosan salts were analyzed, we were also able to follow the formation of AgNPs by their SPR (Figs. 3 and 4). The CHT1S solution was less viscous than its parent solution, and the formation of AgNPs was followed for more extended periods of time.

The UV–Vis spectra of all samples were processed with the Origin software to smooth the curves (see supporting information for more details) and adequately determine the Intensity of the Extinction Maximum (IEM), the Wavelength value of the Extinction Maximum (WEM), and the degree of asymmetry (RL/RW ratio) of the SPR peak by assessing the Half Height Width on the left (LW) and on the right (RW) for the Full Width at the Half Maximum (FWHM) [35]. Values of IEM, WEM, and RW/RL ratio are summarized in Tables 1-4S in the supporting information. These analyses allowed us to determine the effect of reaction time, polymer type, and silver concentration on the features of the silver nanoparticles.

In all cases, IEM values increased with concentration and time, as expected, since this value is related to the amount of AgNPs in the solution, which is expected to increase with both parameters [35]. The position of the typical SPR of silver nanoparticles (WEN) depended on the polymer used, chitosan or salt, and the molecular weight of the sample. At high Mw, both chitosan and chitosan salt (CHT1 and CHT1S)

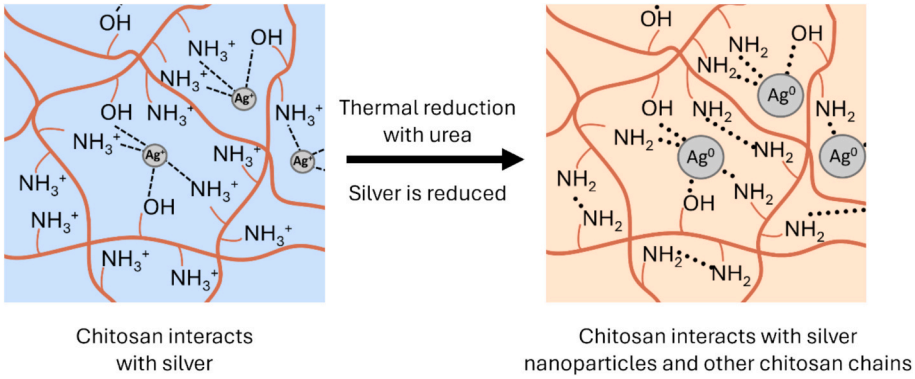

Scheme 1. Schematic representation of the crosslinked phenomena in chitosan silver solution heated in the presence of urea.

Table 3
Gelling time of chitosan-urea solutions with and without $AgNO_3$ and maximum viscosity reached by the hydrogels in each case.

Sample	Gelling time (min)	Max. viscosity (cP)
CHT1	170	2.63 ± 0.27
CHT1 + 40 mM $AgNO_3$	93	256.72 ± 35.66
CHT2	355	1.55 ± 0.17
CHT2 + 40 mM $AgNO_3$	260	3.79 ± 0.27
CHT1S	285	1.18 ± 0.07
CHT1S + 40 mM $AgNO_3$	146	49.73 ± 6.71
CHT2S	360	1.62 ± 0.11
CHT2S + 40 mM $AgNO_3$	260	10.18 ± 1.26

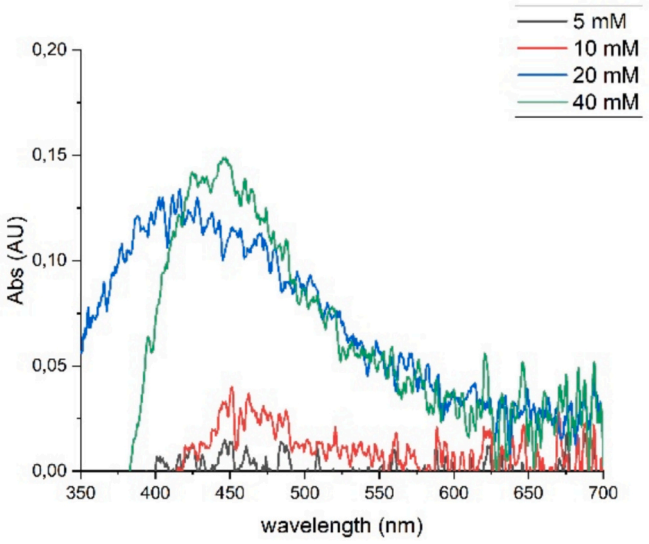

Fig. 1. AgNPs SPR measurements during the formation of CHT1 hydrogel for different silver concentrations at 60 min.

showed a decrease in WEM as the silver concentration increased. In contrast, the low-molecular-weight sample and its salt exhibited the opposite trend. WEM values were between 400 and 450 nm, which are values larger than those previously reported for small (around 10–15 nm) AgNPs in the presence of chitosan [35,53]. This is expected for samples CHT1 and CHT2 since they were not able to stabilize AgNPs produced in the thermal procedure and no SPR was observed. The presence of SPR at 60 min indicates that both the increase in pH and viscosity are improving the stabilization of AgNPs. In the case of salt samples, the spectra were similar to those previously reported for the production of AgNPs in solution [26]. The analysis of band symmetry revealed that the RW/RL ratio tends to decrease as the silver concentration increases in both low-molecular-weight chitosan and chitosan salts. The reduction of RW/RL ratio has been interpreted as an indicator of the rise of the number of nanoparticles with a size below 30 nm [35]. A RW/RL ratio that tends to one is related to an increase in the spectra symmetry, which is related to a narrower size distribution [53].

To further confirm the presence of AgNPs in the hydrogels, high-molecular-weight samples (CHT1 and CHT1S) at different silver concentrations were evaluated under TEM (Figs. 5 and 6). For comparative purposes with UV–Vis data, samples were analyzed at the same time as the last measurement from UV–vis was taken (Fig. 5).

In good agreement with the presence of the SPR band during chitosan hydrogel formation, silver AgNPs were detected not only in the sulfated derivative but also in the parent chitosan. In all samples, the presence of pseudospherical nanoparticles was observed. AgNPs produced with chitosan exhibited larger sizes with a broad distribution. When the chitosan salt was used, the size of the AgNPs was reduced and a narrower particle distribution was estimated from the ImageJ tool (Fig. 2S). These results are in good agreement with the SPR spectra of the samples.

The shape and size of the AgNPs once the hydrogel was produced were also studied (Fig. 6). Again, pseudospherical nanoparticles were observed. The size and polydispersity of the nanoparticles were estimated using the ImageJ tool (Fig. 3S). The nanoparticle size in the chitosan samples was centered around 6 nm with low polydispersity. In the case of samples from CHT1S chitosan, the AgNPs were smaller in size (centered around 3 nm) except for the silver concentration of 40 mM. In the sample with the higher silver concentration, the particle size was centered around 12 nm. This result is not in agreement with the data from the spectral studies and previous TEM images in the liquid state, where larger sizes were determined. This can be explained by considering that the formation was monitored using UV–Vis spectroscopy for 100 min (Fig. 5), while the entire reaction lasted for 300 min (Fig. 6). As the reaction time passes, the viscosity of the media increases, reducing the mobility of the Ag^+ ion and thus promoting the nucleation over the growth; therefore, the formation of small AgNPs is promoted once the viscosity is high enough to constrain AgNPs movement and the acidity of the media is neutralized. These results demonstrate how the AgNPs environment (viscosity and pH) controls AgNPs nucleation and stabilization.

The presence of silver nanoparticles was further confirmed by the analysis of the Selected Area Electron Diffraction (SAED) pattern and Energy-dispersive X-ray spectroscopy (EDX), as shown in Fig. 7. The EDX analysis reveals the presence of silver in the hydrogels, while the SAED pattern indicates the presence of crystalline planes (111 and 220) belonging to silver nanoparticles.

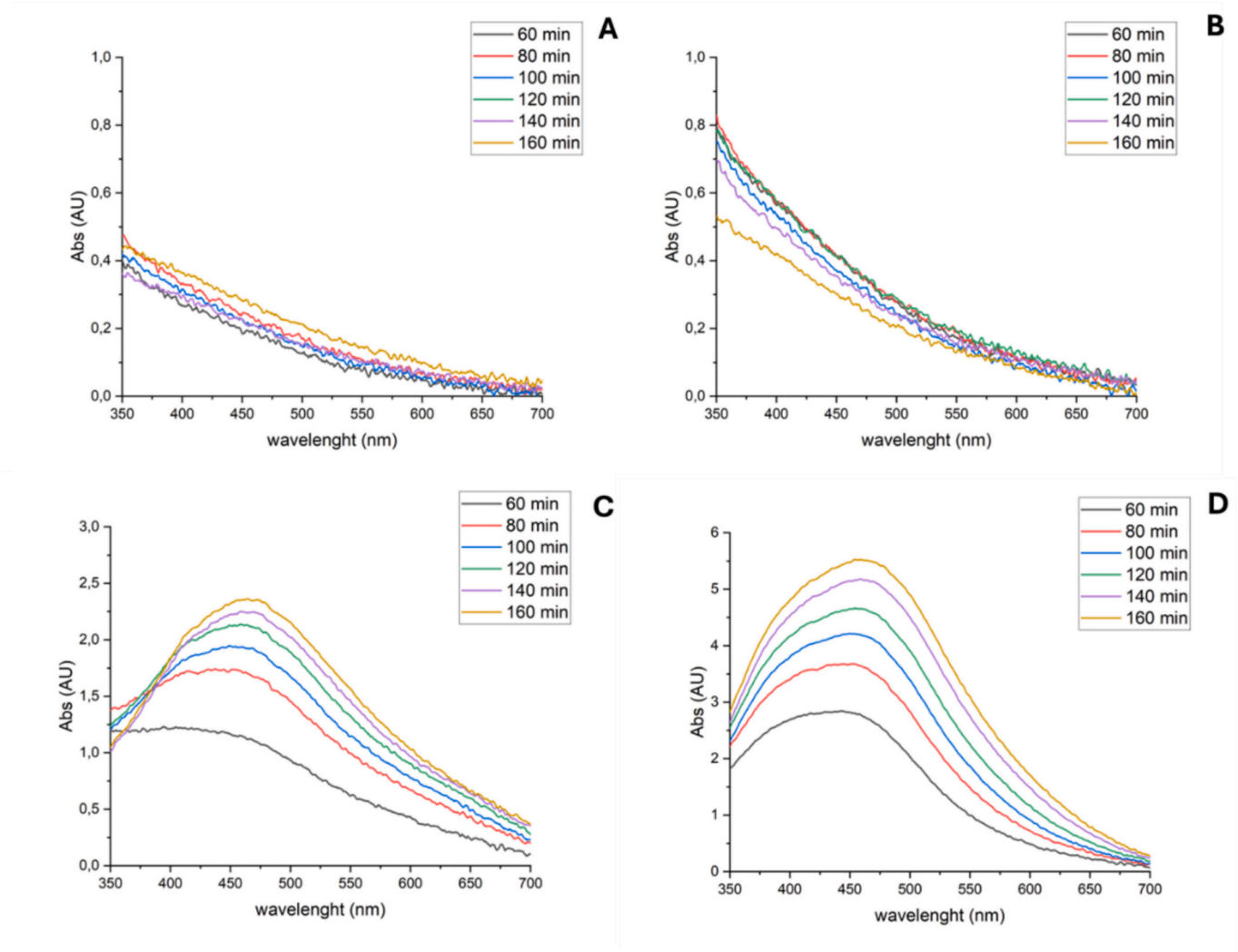

Fig. 2. AgNPs SPR measurements over time during the formation of CHT2 hydrogel at different silver concentrations: A) 5 mM, B) 10 mM, C) 20 mM, and D) 40 mM.

4. Biological characterization

4.1. Antioxidant activity

In normal wound healing, low levels of reactive oxygen species and oxidative stress are desirable. However, an excess of this oxidative process harms wound healing. Therefore, antioxidants may help to control the oxidative process and accelerate wound healing [54]. DPPH and FRAP assays were performed on the samples to evaluate their antioxidant activity. The DPPH assay evaluates the ability of a compound to neutralize free radicals, whereas the FRAP assay relies on the ability of antioxidants to reduce Fe^{3+} to Fe^{2+}.

Initially, we assayed the antioxidant activity of the polymers without silver nanoparticles at a polymer concentration of 1, 5, and 10 mg/mL as a control. For the FRAP analysis, the sample's antioxidant activity was measured using Trolox as a standard (Fig. 3S). The results showed that the activity depended on both the polymer properties and its concentration. Chitosan salts exhibited lower activity than their parent chitosans, and the sample with the highest molecular weight showed the highest activity. However, in all cases, the antioxidant activity was low, indicating that the polymers *per se* have little antioxidant activity. Moreover, the percentage of DPPH inhibition was almost negligible in the polymers (data not shown), which supports the low antioxidant activity exhibited by the polymers.

The antioxidant activity of formulations containing silver at varying concentrations was also assessed using FRAP and DPPH assays (Table 4). In the FRAP assay, at low silver concentrations, the antioxidant effect was comparable to that of control samples without silver. At a silver concentration of 40 mM, the activity was higher, particularly in samples produced with chitosan, which nearly doubled the value compared to the salts. In the DPPH assay, moderate antioxidant activity was observed in the samples, with a maximum inhibition percentage of approximately 5 %. In both assays, the antioxidant activity was lower than in other previously published [28,55,56]. This can be explained by considering two questions. Firstly, polyphenols with potent antioxidant activity are frequently used as reducing agents for the production of AgNPs, so we hypothesized that the antioxidant activity described in these articles came not only from the AgNPs but also from those polyphenols, which are well-known antioxidant molecules. Secondly, antioxidant activity depends on AgNPs concentration, as observed when comparing 5 mm and 40 mM samples (Table 4) and previously reported [28,57]. Unfortunately, from the data found in these articles that solely use chitosan as a reductant and stabilizer, no data is available to calculate the amount of silver tested. For instance, Dara et al. reported a 10-fold increase in the observed values in the DPPH assay between the control and silver-containing composites [28]. Moreover, Shehabeldine et al. reported that a minimum amount of composite (31,25 μg/mL) is needed to start detecting the antioxidant activity in the DPPH assay. Therefore, we consider that the low activity detected is also related to the amount of sample assayed, as increases of around 2.5- to 8.5-fold and 1.7- to 5.2-

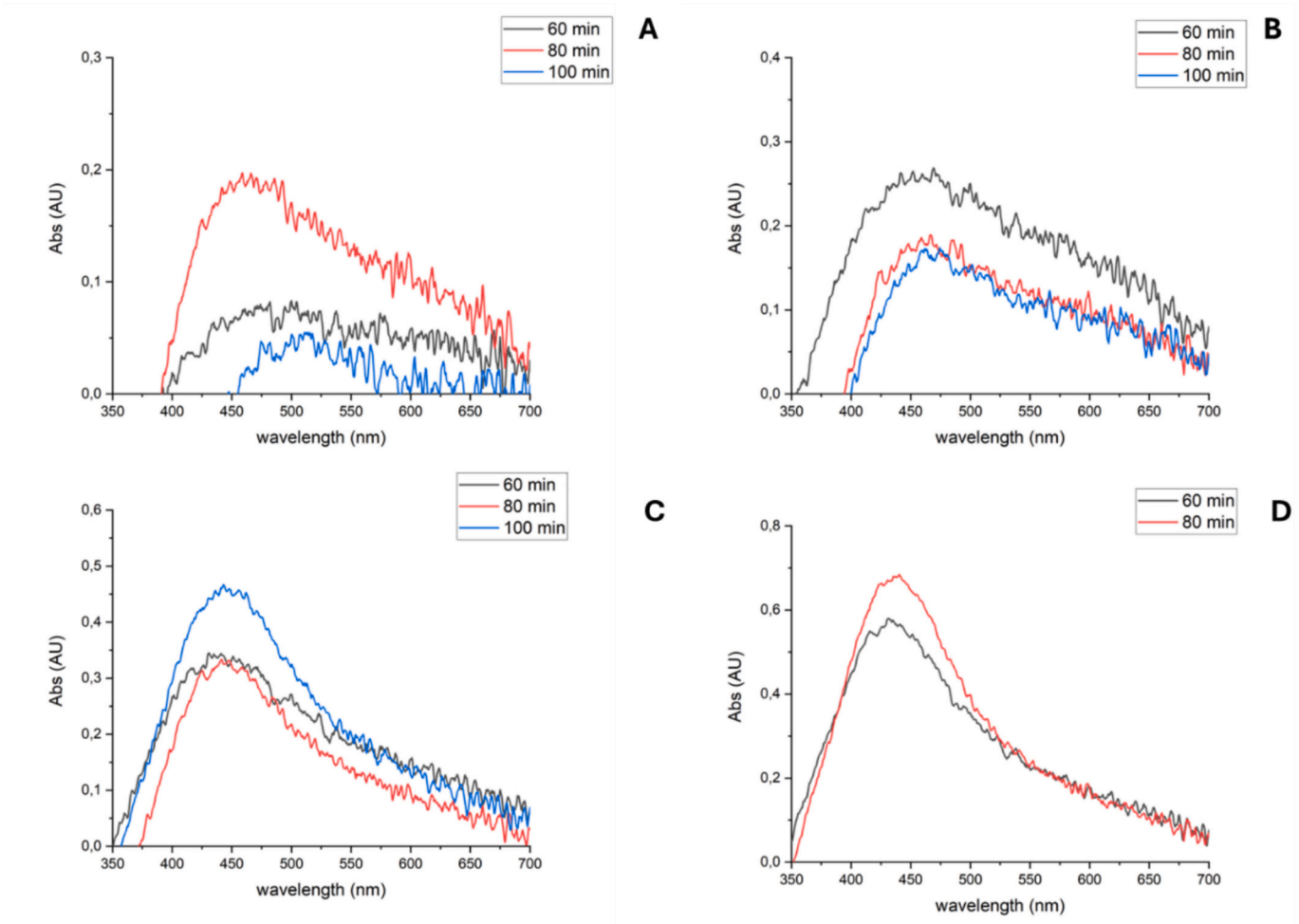

Fig. 3. AgNPs SPR measurements over time during the formation of CHT1S hydrogel at different silver concentrations: A) 5 mM, B) 10 mM, C) 20 mM, and D) 40 mM.

fold were found in FRAP and DPPH assays, respectively, when the silver concentration was increased from 5 to 40 mM.

4.2. Antimicrobial activity

The antimicrobial activity of AgNP-chitosan-based hydrogels was determined against two clinically relevant pathogens associated with wound healing (*E. coli* and *S. aureus*). The results, presented in Table 5, demonstrate that all formulations containing silver nanoparticles exhibit antimicrobial activity against both bacterial strains. The level of inhibition was dependent on the concentration of silver, the type of chitosan used, and the bacterium tested. In contrast, the control samples did not produce any zone of inhibition (ZOI). In general, inhibition zones were larger in *E. coli* compared to *S. aureus* using the same AgNPs concentration and polymer.

In *E. coli*, slight differences were observed between the different samples at the same silver concentration, depending on the polymer used to produce the AgNPs. At a low silver concentration (5 mM), the CHT1S formulation exhibited higher activity than the others; this activity was not affected by the silver concentration (a constant ZOI of 11.5 mm was observed at all concentrations), and this difference disappeared at higher concentrations. This behavior may indicate that silver release from the CHT1S hydrogel has a saturation point at low concentrations, such that at higher concentrations no further advantage is achieved in terms of diffusion or antibacterial activity. The other samples exhibited a behavior not directly related to silver concentration, with maximum activity achieved at varying concentrations. In sample CHT 1, maximum activity was observed in the 10–20 mM range, while at higher concentrations, a reduction in ZOI was noted. Similarly, in sample CHT2, the maximum was achieved at 20 mM, and a decrease in ZOI was observed at higher concentrations. In sample CHT2S, the maximum was reached in the range 20–40 mM. CHT2S exhibited a concentration-dependent antimicrobial effect, where the zone of inhibition increased to a diameter of 13 mm at 40 mM $AgNO_3$, whereas it was a minimum of 9.5 mm at 5 mM $AgNO_3$. This tendency suggests that the structure of CHT2S is relatively easy to lose, leading to the release of Ag ions.

Although one should expect an increase in the activity as silver concentration increases, this behavior has been previously observed by other authors [58]. This can be attributed to a lower diffusion of silver in the agar media at high silver concentrations or to less accessible silver in the hydrogels as the silver concentration increases, due to a more compact hydrogel structure produced by a denser crosslinked structure.

In *S. aureus*, the antimicrobial activity was also affected not only by silver concentration but also by the polymer nature (chitosan or chitosan salts). When comparing sample CHT2 with CHT2S, we observed that at a low silver concentration, the salt did not produce a zone of inhibition. However, this sample had the largest ZOI at a high silver concentration. Contrary to *E. coli*, in this strain, an increase in silver concentration was followed by a rise in ZOI; therefore, *S. aureus* appears to be more sensitive to AgNPs concentration within the chitosan-based hydrogels than *E. coli*. In fact, in some formulations at 40 mM, ZOI is slightly larger for

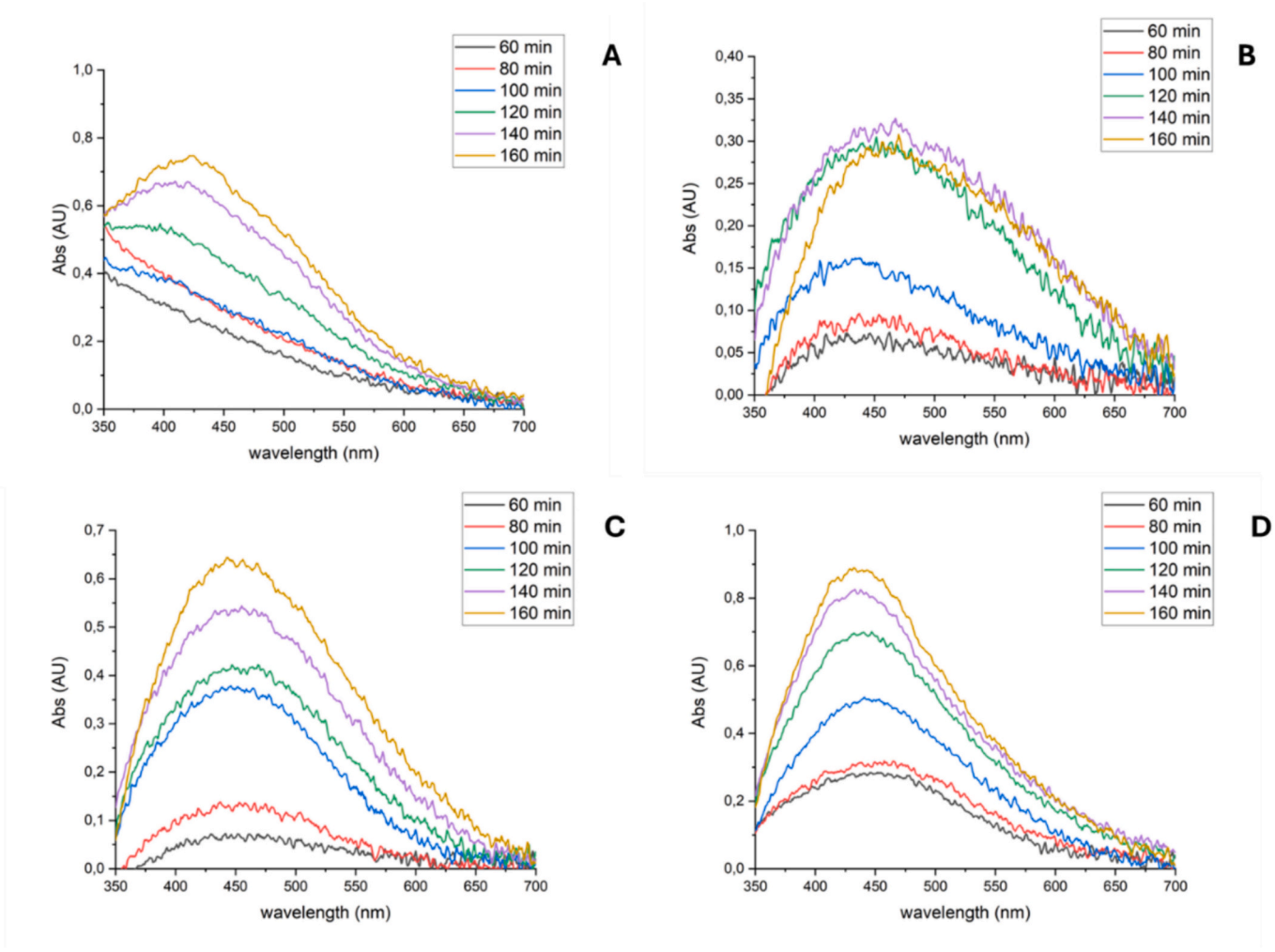

Fig. 4. AgNPs SPR measurements over time during the formation of CHT2S hydrogel at different silver concentrations: A) 5 mM, B) 10 mM, C 20 mM, and D) 40 mM.

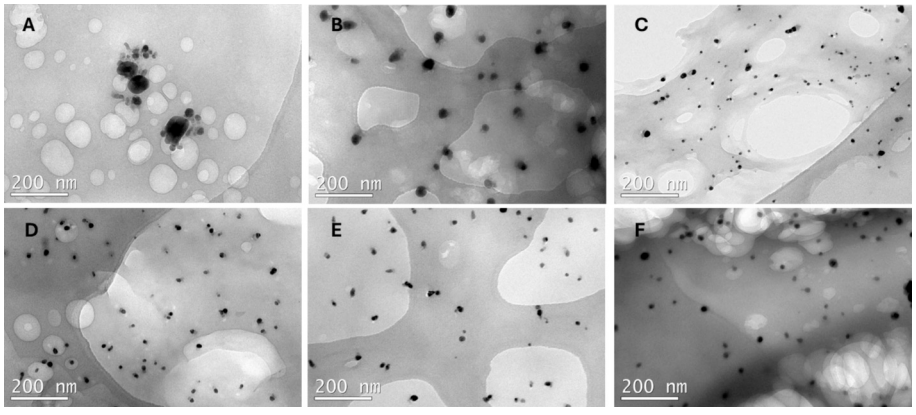

Fig. 5. TEM images of AgNPs formed within the chitosan (up panel) and chitosan salt (down).

S. aureus than for *E. coli*. This result is not typical, as *E. coli* tends to be more sensitive to AgNPs than *S. aureus* due to differences in the cell wall structure. The thinner peptidoglycan layer of Gram-negative bacteria facilitates easier penetration of AgNPs compared to the thicker wall of Gram-positive bacteria, such as *S. aureus* [59,60]. Although our results are not typical, other authors have described a similar behavior [61,62]. In previous works, different AgNPS hydrogels have been tested against *E. coli* and *S. aureus*. For example, ultrasmall AgNPs in pluronic hydrogels tested against (*E. coli* 10P50 and *S. aureus* ATCC 25923) showed ZOI of 18 and 12 mm, respectively. In the case of *S. aureus*, the value falls within the range obtained in this work and is slightly smaller in the case of *E. coli*; however, a different collection strain was used in this case [63]. In another example, AgNPS composite hydrogels of silk fibroin stabilized with Carboxymethyl Cellulose-Na exhibited a ZOI of around 6.0 mm and 2.5 mm when tested against *S. aureus* (ATCC 29737) and *E. coli* (ATCC 25922), respectively [64].In the case of AgNPs

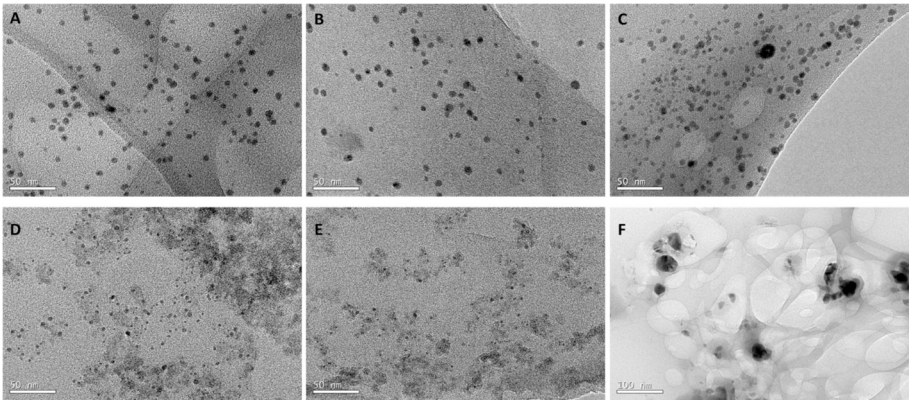

Fig. 6. TEM images of AgNps formed within the chitosan (up panel) and chitosan salt (down panel) at a silver concentration of 10 (A, D), 20 (B, E), and 40 mM (C, F) after hydrogel formation.

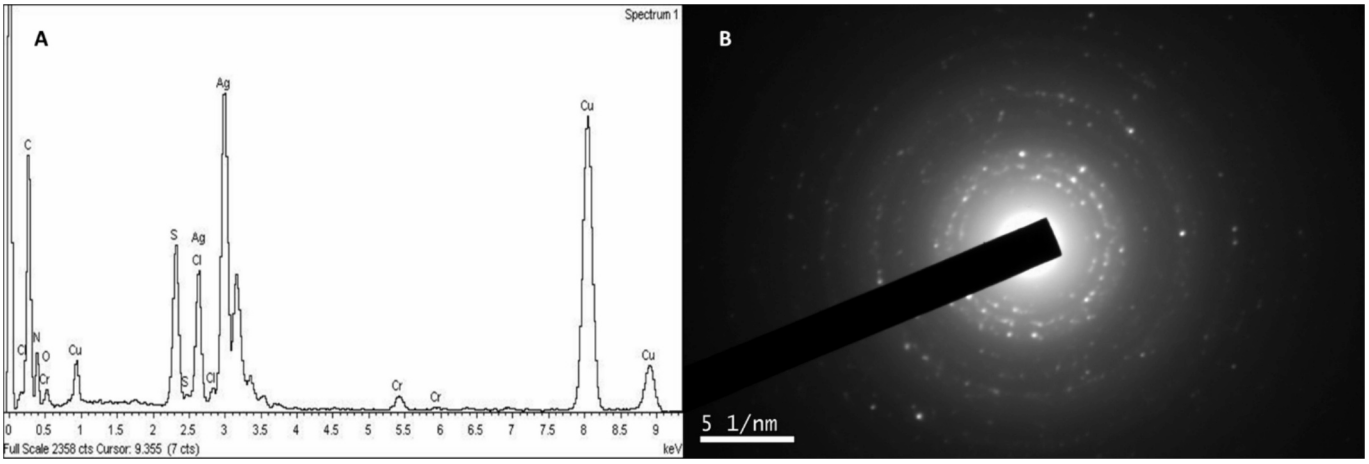

Fig. 7. EDX and SAED pattern of AgNPs produced by sample CHT1S.

Table 4
Antioxidant activity of silver-containing samples by FRAP and DPPH methods.

Sample	FRAP		DPPH	
	Trolox, mM		Inhibition, %	
	AgNPs, 5 mM	AgNPs, 40 mM	AgNPs, 5 mM	AgNPs, 40 mM
CHT1	0.059 ± 0.009	0.394 ± 0.086	n.d.	2.79 ± 0.59
CHT1S	0.013 ± 0.0.005	0.198 ± 0.056	n.d.	1.72 ± 0.67
CHT2	0.030 ± 0.001	0.472 ± 0.035	n.d.	5.18 ± 1.23
CHT2S	0.017 ± 0.005	0.267 ± 0.033	n.d.	2.08 ± 0.65

saponine nanocomposites ZOI between 6.67 and 20.00 mm and 7.33–23.50 mm were determined for *E. coli* (ATCC 25922) and *S. aureus* (ATCC 11632), respectively [58]. In this example, different AgNPs loadings were tested, showing that the activity was not directly related to the AgNPs concentrations. Although it is difficult to directly compare the different formulations, since activity is not always directly associated with silver load and there is no homogeneity in the source of collection of the strains selected, our results are in good agreement with previous works showing that AgNPs hydrogels are promising materials for avoiding bacterial contamination in wound healing.

5. Conclusions

In this paper, we describe a one-pot procedure to produce silver nanoparticles inside a chitosan or chitosan salt hydrogel formed by the thermal decomposition of urea, during which silver nanoparticles are also produced. This approach represents a significant improvement over previously multistep methods for preparing silver nanoparticles in

Table 5
Antimicrobial activity of AgNPs-hydrogels against *E. coli and S. aureus*.

Inhibition diameter, mm								
Sample	CHT1[a]	CHT1[b]	CHT2[a]	CHT2[b]	CHT1S[a]	CHT1S[b]	CHT2S[a]	CHT2S[b]
Control	0.0 ± 0.0	0.0 ± 0.0	0.0 ± 0.0	0.0 ± 0.0	0.0 ± 0.0	0.0 ± 0.0	0.0 ± 0.0	0.0 ± 0.0
5 mM $AgNO_3$	9.0 ± 0.0	8.0 ± 0.0	8.5 ± 2.1	8.0 ± 1.4	11.5 ± 0.0	9.5 ± 0.7	9.5 ± 0.7	0.0 ± 0.0
10 mM $AgNO_3$	12.0 ± 0.0	9.5 ± 0.7	10.5 ± 0.7	9.5 ± 0.7	11.5 ± 0.7	9.5 ± 0.7	9.5 ± 0.7	10.0 ± 0.0
20 mM $AgNO_3$	11.0 ± 1.4	10.0 ± 0.0	12.0 ± 0.0	10.0 ± 0.0	11.5 ± 0.7	10.0 ± 0	12 ± 2.8	10.5 ± 0.7
40 mM $AgNO_3$	10.0 ± 0.0	11.0 ± 0.0	9.0 ± 0.0	10.5 ± 0.7	11.5 ± 0.7	11.5 ± 0.7	13 ± 1.4	14.0 ± 1.4

[a] *E. coli* assay and
[b] *S. aureus* assay.

hydrogels since it can be used over a variety of chitosan samples, including those that, *per se*, are not able to stabilize AgNPs and simplifies the process. Viscometric measurement of the gelation kinetics revealed that the gelling time of the silver-chitosan solutions decreased with increasing silver concentration, attributed to intermolecular cross-linking between silver ions and chitosan. This new methodology enabled us to better control the stabilization of AgNPs produced by chitosan, due to the increased viscosity during the gelation process and the controlled increase in pH, from acidic to basic. Moreover, the generated environment favors nanoparticle nucleation over aggregation. These results demonstrate how the AgNPs environment (viscosity and pH) controls AgNPs nucleation and stabilization.

The formed hydrogels exhibited moderate antioxidant activity in the DPPH and FRAP tests, with this activity being concentration dependent. Antimicrobial assessment against *Escherichia coli* ATCC 25922 and *Staphylococcus aureus* ATCC 25923 demonstrated significant antibacterial activity of all silver-containing samples, whereas no inhibition was observed for the control hydrogels without silver. This biocompatible method yields the production of AgNP-chitosan hydrogels, with potential applications in wound care where both antimicrobial protection and oxidative stress reduction are crucial. In particular, sulfated samples produced chitosan hydrogels in the form of small gel fragments that can be applied to fill irregular wounds with tissue loss.

CRediT authorship contribution statement

S. Pouri: Writing – review & editing, Methodology, Investigation, Formal analysis, Data curation. **I. Fraile-Gutiérrez:** Writing – review & editing, Methodology, Investigation, Formal analysis, Data curation. **R. Gil-Gonzalo:** Writing – review & editing, Investigation, Formal analysis. **N. Acosta:** Writing – review & editing, Supervision, Formal analysis. **F. Navarro-García:** Writing – review & editing, Supervision, Resources, Formal analysis. **I. Aranaz:** Writing – review & editing, Writing – original draft, Visualization, Supervision, Methodology, Investigation, Funding acquisition, Formal analysis, Conceptualization.

Declaration of competing interest

The authors declare that they have no known competing financial interests or personal relationships that could have appeared to influence the work reported in this paper.

Acknowledgments

R.G-G acknowledges a grant from Garantía Juvenil Program (Yo Investigo) supported by MICIU/AEI/10.13039/501100011033. Financial support from Project PID2021-123045OB-I00 supported by MICIU/AEI/10.13039/501100011033 is also acknowledged.

Appendix A. Supplementary data

Supplementary data to this article can be found online at https://doi.org/10.1016/j.ijbiomac.2025.148655.

Data availability

Data will be made available on request.

References

[1] M.A. Dheyab, N. Oladzadabbasabadi, A.A. Aziz, P.M. Khaniabadi, M.T.S. Al-ouqaili, M.S. Jameel, F.S. Braim, B. Mehrdel, M. Ghasemlou, Recent advances of plant-mediated metal nanoparticles: synthesis, properties, and emerging applications for wastewater treatment, J. Environ. Chem. Eng. 12 (2024), https://doi.org/10.1016/j.jece.2024.112345.

[2] W.H. Elmer, J.C. White, The use of metallic oxide nanoparticles to enhance growth of tomatoes and eggplants in disease infested soil or soilless medium, Environ. Sci. Nano. 3 (2016) 1072–1079, https://doi.org/10.1039/c6en00146g.

[3] A. Llorens, E. Lloret, P.A. Picouet, R. Trbojevich, A. Fernandez, Metallic-based micro and nanocomposites in food contact materials and active food packaging, Trends Food Sci. Technol. 24 (2012) 19–29, https://doi.org/10.1016/j.tifs.2011.10.001.

[4] M. Mesgari, A.H. Aalami, A. Sahebkar, Antimicrobial activities of chitosan/titanium dioxide composites as a biological nanolayer for food preservation: a review, Int. J. Biol. Macromol. 176 (2021) 530–539, https://doi.org/10.1016/j.ijbiomac.2021.02.099.

[5] L.M. Shaker, A.A. Al-Amiery, W.K. Al-Azzawi, Nanomaterials: paving the way for the hydrogen energy frontier, Discov. Nano. 19 (2024), https://doi.org/10.1186/s11671-023-03949-8.

[6] M.R. El-Aassar, O.M. Ibrahim, M.M.G. Fouda, N.G. El-Beheri, M.M. Agwa, Wound healing of nanofiber comprising polygalacturonic/hyaluronic acid embedded silver nanoparticles: in-vitro and in-vivo studies, Carbohydr. Polym. 238 (2020), https://doi.org/10.1016/j.carbpol.2020.116175.

[7] F.U. Khan, Y. Chen, N.U. Khan, Z.U.H. Khan, A.U. Khan, A. Ahmad, K. Tahir, L. Wang, M.R. Khan, P. Wan, Antioxidant and catalytic applications of silver nanoparticles using Dimocarpus longan seed extract as a reducing and stabilizing agent, J. Photochem. Photobiol. B Biol. 164 (2016) 344–351, https://doi.org/10.1016/j.jphotobiol.2016.09.042.

[8] G.R. Khayati, K. Janghorban, The nanostructure evolution of Ag powder synthesized by high energy ball milling, Adv. Powder Technol. 23 (2012) 393–397, https://doi.org/10.1016/j.apt.2011.05.005.

[9] Y. Gafner, D.A. Ryzhkova, S.L. Gafner, D.G. Gromov, S.V. Dubkov, D.V. Novikov, N.I. Borgardt, R.L. Volkov, G.M. Poletaev, Determination of structural features of silver nanoparticles synthesized by vacuum thermal evaporation on a carbon substrate, Mater. Chem. Phys. 326 (2024) 129810, https://doi.org/10.1016/j.matchemphys.2024.129810.

[10] M. (Wabwile) Juma, M.M. Nancy, Z. Birech, A. Moraa Ondieki, M. Maaza, D. Mkhoztwa, Using laser ablation in liquid (LASIS) method to synthesize silver nanoparticles for SERS applications, Mater. Today Proc. (2023), https://doi.org/10.1016/j.matpr.2023.07.372.

[11] N. Abid, A.M. Khan, S. Shujait, K. Chaudhary, M. Ikram, M. Imran, J. Haider, M. Khan, Q. Khan, M. Maqbool, Synthesis of nanomaterials using various top-down and bottom-up approaches, influencing factors, advantages, and disadvantages: a review, Adv. Colloid Interf. Sci. 300 (2022) 102597, https://doi.org/10.1016/j.cis.2021.102597.

[12] H. Alsubaie, Z. Zaheer, E.S. Aazam, Role of ionic surfactants on the nucleation and growth of silver nanoparticles, J. Mol. Liq. 341 (2021) 117309, https://doi.org/10.1016/j.molliq.2021.117309.

[13] A. Castonguay, A.K. Kakkar, Dendrimer templated construction of silver nanoparticles, Adv. Colloid Interf. Sci. 160 (2010) 76–87, https://doi.org/10.1016/j.cis.2010.07.006.

[14] D. Debnath, Y. Lee, K.E. Geckeler, Biocompatible polymers as a tool for the synthesis of silver nanoparticles: size tuning and in vitro cytotoxicity studies, Polym. Int. 66 (2017) 512–520, https://doi.org/10.1002/pi.5304.

[15] H. Huang, X. Yang, Synthesis of polysaccharide-stabilized gold and silver nanoparticles:a green method, Carbohydr. Res. 339 (2004) 2627–2631, https://doi.org/10.1016/j.carres.2004.08.005.

[16] H. Kang, J.T. Buchman, R.S. Rodriguez, H.L. Ring, J. He, K.C. Bantz, C.L. Haynes, Stabilization of silver and gold nanoparticles: preservation and improvement of plasmonic functionalities, Chem. Rev. 119 (2019) 664–699, https://doi.org/10.1021/acs.chemrev.8b00341.

[17] B. Lu, F. Lu, Y. Zou, J. Liu, B. Rong, Z. Li, F. Dai, D. Wu, G. Lan, In situ reduction of silver nanoparticles by chitosan-L-glutamic acid/hyaluronic acid: enhancing antimicrobial and wound-healing activity, Carbohydr. Polym. 173 (2017) 556–565, https://doi.org/10.1016/j.carbpol.2017.06.035.

[18] M. Mahmood, M. Abid, M.F. Nazar, M.N. Zafar, M.A. Raza, M. Ashfaq, A.M. Khan, S.H. Sumrra, M. Zubair, The wet chemical synthesis of surfactant-capped quasi-spherical silver nanoparticles with enhanced antibacterial activity, Mater. Adv. 1 (2020) 2332–2338, https://doi.org/10.1039/D0MA00408A.

[19] Y. Murali Mohan, K. Vimala, V. Thomas, K. Varaprasad, B. Sreedhar, S.K. Bajpai, K. Mohana Raju, Controlling of silver nanoparticles structure by hydrogel networks, J. Colloid Interface Sci. 342 (2010) 73–82, https://doi.org/10.1016/j.jcis.2009.10.008.

[20] K. Vimala, K. Samba Sivudu, Y. Murali Mohan, B. Sreedhar, K. Mohana Raju, Controlled silver nanoparticles synthesis in semi-hydrogel networks of poly (acrylamide) and carbohydrates: a rational methodology for antibacterial application, Carbohydr. Polym. 75 (2009) 463–471, https://doi.org/10.1016/j.carbpol.2008.08.009.

[21] R. Begum, G. Ahmad, J. Najeeb, W. Wu, A. Irfan, M. Azam, J. Nisar, Z.H. Farooqi, Stabilization of silver nanoparticles in crosslinked polymer colloids through chelation for catalytic degradation of p-nitroaniline in aqueous medium, Chem. Phys. Lett. 763 (2021) 138263, https://doi.org/10.1016/j.cplett.2020.138263.

[22] M. Kołodziejska, K. Jankowska, M. Klak, M. Wszola, Chitosan as an underrated polymer in modern tissue engineering, Nanomaterials 11 (2021) 3019, https://doi.org/10.3390/nano11113019.

[23] The United States Pharmacopeia 34 / National Formulary 29, 2011.

[24] N.M. Zain, A.G.F. Stapley, G. Shama, Green synthesis of silver and copper nanoparticles using ascorbic acid and chitosan for antimicrobial applications, Carbohydr. Polym. 112 (2014) 195–202, https://doi.org/10.1016/j.carbpol.2014.05.081.

[25] A. Shah, I. Hussain, G. Murtaza, Chemical synthesis and characterization of chitosan/silver nanocomposites films and their potential antibacterial activity, Int. J. Biol. Macromol. 116 (2018) 520–529, https://doi.org/10.1016/j.ijbiomac.2018.05.057.
[26] I. Aranaz, F. Navarro-García, M. Morri, N. Acosta, L. Casettari, A. Heras, Evaluation of chitosan salt properties in the production of AgNPs materials with antibacterial activity, Int. J. Biol. Macromol. 235 (2023) 123849, https://doi.org/10.1016/j.ijbiomac.2023.123849.
[27] I. Aranaz, C. Castro, A. Heras, N. Acosta, On the ability of low molecular weight chitosan enzymatically depolymerized to produce and stabilize silver nanoparticles, Biomimetics 3 (2018), https://doi.org/10.3390/biomimetics3030021.
[28] P.K. Dara, R. Mahadevan, P.A. Digita, S. Visnuvinayagam, L.R.G. Kumar, S. Mathew, C.N. Ravishankar, R. Anandan, Synthesis and biochemical characterization of silver nanoparticles grafted chitosan (Chi-Ag-NPs): in vitro studies on antioxidant and antibacterial applications, SN Appl. Sci. 2 (2020) 665, https://doi.org/10.1007/s42452-020-2261-y.
[29] L.-S. Wang, C.-Y. Wang, C.-H. Yang, C.-L. Hsieh, S.-Y. Chen, C.-Y. Shen, J.-J. Wang, K.-S. Huang, Synthesis and anti-fungal effect of silver nanoparticles-chitosan composite particles, Int. J. Nanomedicine 10 (2015) 2685–2696, https://doi.org/10.2147/IJN.S77410.
[30] W. Cao, J. Yan, C. Liu, J. Zhang, H. Wang, X. Gao, H. Yan, B. Niu, W. Li, Preparation and characterization of catechol-grafted chitosan/gelatin/modified chitosan-AgNP blend films, Carbohydr. Polym. 247 (2020) 116643, https://doi.org/10.1016/j.carbpol.2020.116643.
[31] S.J. de M. Alves, M.A. Santos, J.E. da S. Neto, H.N. da Silva, M.C.S. Barbosa, M.V. L. Fook, R.F. Navarro, S.M. de L. Silva, Combined effect of pH and neutralizing solution molarity on the rheological properties of chitosan hydrogels for biomedical applications, Gels (Basel). 11 (2025), https://doi.org/10.3390/gels11030212.
[32] C. Schatz, C. Pichot, T. Delair, C. Viton, A. Domard, Static light scattering studies on chitosan solutions: from macromolecular chains to colloidal dispersions, Langmuir 19 (2003) 9896–9903, https://doi.org/10.1021/la034410n.
[33] N. Guerrero-Alburquerque, S. Zhao, N. Adilien, M.M. Koebel, M. Lattuada, W. J. Malfait, Strong, machinable, and insulating chitosan-urea aerogels: toward ambient pressure drying of biopolymer aerogel monoliths, ACS Appl. Mater. Interfaces 12 (2020) 22037–22049, https://doi.org/10.1021/acsami.0c03047.
[34] M.J. Hortigüela, M.C. Gutiérrez, I. Aranaz, M. Jobbágy, A. Abarrategi, C. Moreno-Vicente, A. Civantos, V. Ramos, J.L. López-Lacomba, M.L. Ferrer, F. Del Monte, Urea assisted hydroxyapatite mineralization on MWCNT/CHI scaffolds, J. Mater. Chem. 18 (2008), https://doi.org/10.1039/b815401e.
[35] O.A. Douglas-Gallardo, C.A. Christensen, M.C. Strumia, M.A. Pérez, C.G. Gomez, Physico-chemistry of a successful micro-reactor: random coils of chitosan backbones used to synthesize size-controlled silver nanoparticles, Carbohydr. Polym. 225 (2019) 115241, https://doi.org/10.1016/j.carbpol.2019.115241.
[36] J. Piquero-Casals, D. Morgado-Carrasco, C. Granger, C. Trullàs, A. Jesús-Silva, J. Krutmann, Urea in dermatology: a review of its emollient, moisturizing, keratolytic, skin barrier enhancing and antimicrobial properties, Dermatol. Ther. (Heidelb). 11 (2021) 1905–1915, https://doi.org/10.1007/s13555-021-00611-y.
[37] N. Sereni, A. Enache, G. Sudre, A. Montembault, C. Rochas, P. Durand, M.-H. Perrard, G. Bozga, J.-P. Puaux, T. Delair, L. David, Dynamic structuration of physical chitosan hydrogels, Langmuir 33 (2017) 12697–12707, https://doi.org/10.1021/acs.langmuir.7b02997.
[38] Z. Lu, L. Zou, X. Zhou, D. Huang, Y. Zhang, High strength chitosan hydrogels prepared from NaOH/urea aqueous solutions: the role of thermal gelling, Carbohydr. Polym. 297 (2022) 120054, https://doi.org/10.1016/j.carbpol.2022.120054.
[39] G.G. Allan, M. Peyron, Molecular weight manipulation of chitosan I: kinetics of depolymerization by nitrous acid, Carbohydr. Res. 277 (1995) 257–272, https://doi.org/10.1016/0008-6215(95)00207-A.
[40] A. Heydari, M. Darroudi, I. Lacík, Efficient N-sulfopropylation of chitosan with 1,3-propane sultone in aqueous solutions: neutral pH as the key condition, React. Chem. Eng. 6 (2021) 2146–2158, https://doi.org/10.1039/d1re00089f.
[41] R.A.A.A.A. Muzzarelli, R. Rochetti, V. Stanic, M. Weckx, R. Roccheti, V. Stanic, M. Weckx, Methods for the determination of the degree of acetylation of chitin and chitosan, in: R.A. Muzarelli, M.G. Peter (Eds.), Chitin Handb., Atec Edizioni, Grottammare, Italy, 1997, pp. 109–119.
[42] K. Shimada, K. Fujikawa, K. Yahara, T. Nakamura, Antioxidative properties of xanthan on the autoxidation of soybean oil in cyclodextrin emulsion, J. Agric. Food Chem. 40 (1992) 945–948, https://doi.org/10.1021/jf00018a005.
[43] C. Guo, J. Yang, J. Wei, Y. Li, J. Xu, Y. Jiang, Antioxidant activities of peel, pulp and seed fractions of common fruits as determined by FRAP assay, Nutr. Res. 23 (2003) 1719–1726, https://doi.org/10.1016/j.nutres.2003.08.005.
[44] CLSI, Performance Standards for Antimicrobial Susceptibility Testing; Twenty-fourth Informational Supplement. CLSI document M100-S24 (ISBN 1-56238-897-5 [Print]; ISBN 1-56238-898-3 [Electronic]), 2014.
[45] M.L. Pita-López, G. Fletes-Vargas, H. Espinosa-Andrews, R. Rodríguez-Rodríguez, Physically cross-linked chitosan-based hydrogels for tissue engineering applications: a state-of-the-art review, Eur. Polym. J. 145 (2021) 110176, https://doi.org/10.1016/j.eurpolymj.2020.110176.
[46] P. Li, J. Zhao, Y. Chen, B. Cheng, Z. Yu, Y. Zhao, X. Yan, Z. Tong, S. Jin, Preparation and characterization of chitosan physical hydrogels with enhanced mechanical and antibacterial properties, Carbohydr. Polym. 157 (2017) 1383–1392, https://doi.org/10.1016/j.carbpol.2016.11.016.
[47] I. Aranaz, M.C. Gutiérrez, L. Yuste, F. Rojo, M.L. Ferrer, F. Del Monte, Controlled formation of the anhydrous polymorph of ciprofloxacin crystals embedded within chitosan scaffolds: study of the kinetic release dependence on crystal size, J. Mater. Chem. 19 (2009), https://doi.org/10.1039/b813156b.
[48] H.Y. Zhou, X.G. Chen, M. Kong, C.S. Liu, D.S. Cha, J.F. Kennedy, Effect of molecular weight and degree of chitosan deacetylation on the preparation and characteristics of chitosan thermosensitive hydrogel as a delivery system, Carbohydr. Polym. 73 (2008) 265–273, https://doi.org/10.1016/j.carbpol.2007.11.026.
[49] J. Yang, M. Shen, T. Wu, Y. Luo, M. Li, H. Wen, J. Xie, Role of salt ions and molecular weights on the formation of Mesona chinensis polysaccharide-chitosan polyelectrolyte complex hydrogel, Food Chem. 333 (2020) 127493, https://doi.org/10.1016/j.foodchem.2020.127493.
[50] M. Kozicki, M. Kołodziejczyk, M. Szynkowska, A. Pawlaczyk, E. Leśniewska, A. Matusiak, A. Adamus, A. Karolczak, Hydrogels made from chitosan and silver nitrate, Carbohydr. Polym. 140 (2016) 74–87, https://doi.org/10.1016/j.carbpol.2015.12.017.
[51] W.-F. Lee, K.-T. Tsao, Effect of silver nanoparticles content on the various properties of nanocomposite hydrogels by in situ polymerization, J. Mater. Sci. 45 (2010) 89–97, https://doi.org/10.1007/s10853-009-3896-7.
[52] Y.-K. Twu, Y.-W. Chen, C.-M. Shih, Preparation of silver nanoparticles using chitosan suspensions, Powder Technol. 185 (3) (2008) 251–257, https://doi.org/10.1016/j.powtec.2007.10.025.
[53] M.R. Romero, N.A. Coser, M.A. Pérez, C.G. Gomez, Poly(N-isopropylacrylamide)-interpenetrated chitosan coils working as nanoreactors for controlled silver nanoparticle growth, Carbohydr. Polym. 288 (2022) 119374, https://doi.org/10.1016/j.carbpol.2022.119374.
[54] S.D. Fitzmaurice, R.K. Sivamani, R.R. Isseroff, Antioxidant therapies for wound healing: a clinical guide to currently commercially available products, Skin Pharmacol. Physiol. 24 (2011) 113–126, https://doi.org/10.1159/000322643.
[55] S. Salari, S. Esmaeilzadeh Bahabadi, A. Samzadeh-Kermani, F. Yosefzaei, In-vitro evaluation of antioxidant and antibacterial potential of greensynthesized silver nanoparticles using prosopis farcta fruit extract, Iran. J. Pharm. Res. IJPR 18 (2019) 430–455.
[56] S. Bhakya, S. Muthukrishnan, M. Sukumaran, M. Muthukumar, Biogenic synthesis of silver nanoparticles and their antioxidant and antibacterial activity, Appl. Nanosci. 6 (2016) 755–766, https://doi.org/10.1007/s13204-015-0473-z.
[57] A.M. Shehabeldine, S.S. Salem, O.M. Ali, K.A. Abd-Elsalam, F.M. Elkady, A. H. Hashem, Multifunctional silver nanoparticles based on chitosan: antibacterial, antibiofilm, antifungal, antioxidant, and wound-healing activities, J. Fungi (Basel, Switzerland) 8 (2022), https://doi.org/10.3390/jof8060612.
[58] M. Sprynskyy, H. Sokol, K. Rafińska, W. Brzozowska, V. Railean-Plugaru, P. Pomastowski, B. Buszewski, Preparation of AgNPs/saponite nanocomposites without reduction agents and study of its antibacterial activity, Colloids Surf. B: Biointerfaces 180 (2019) 457–465, https://doi.org/10.1016/j.colsurfb.2019.04.066.
[59] A. Gibała, P. Żeliszewska, T. Gosiewski, A. Krawczyk, D. Duraczyńska, J. Szaleniec, M. Szaleniec, M. Oćwieja, Antibacterial and antifungal properties of silver nanoparticles—effect of a surface-stabilizing agent, Biomolecules 11 (2021), https://doi.org/10.3390/biom11101481.
[60] S. Akter, M.A. Huq, Biologically rapid synthesis of silver nanoparticles by *Sphingobium* sp. MAH-11T and their antibacterial activity and mechanisms investigation against drug-resistant pathogenic microbes, Artif. Cells Nanomed. Biotechnol. 48 (2020) 672–682, https://doi.org/10.1080/21691401.2020.1730390.
[61] Z. Liu, L. Wang, X. Zhao, Y. Luo, K. Zheng, M. Wu, Highly effective antibacterial AgNPs@hinokitiol grafted chitosan for construction of durable antibacterial fabrics, Int. J. Biol. Macromol. 209 (2022) 963–971, https://doi.org/10.1016/j.ijbiomac.2022.04.103.
[62] M. Alavi, N. Karimi, Antibacterial, hemoglobin/albumin-interaction, and molecular docking properties of phytogenic AgNPs functionalized by three antibiotics of penicillin, amoxicillin, and tetracycline, Microb. Pathog. (2022) 105427, https://doi.org/10.1016/j.micpath.2022.105427.
[63] H. Haidari, Z. Kopecki, R. Bright, A.J. Cowin, S. Garg, N. Goswami, K. Vasilev, Ultrasmall AgNP-impregnated biocompatible hydrogel with highly effective biofilm elimination properties, ACS Appl. Mater. Interfaces 12 (2020) 41011–41025, https://doi.org/10.1021/acsami.0c09414.
[64] R. Raho, N.-Y. Nguyen, N. Zhang, W. Jiang, A. Sannino, H. Liu, M. Pollini, F. Paladini, Photo-assisted green synthesis of silver doped silk fibroin/carboxymethyl cellulose nanocomposite hydrogels for biomedical applications, Mater. Sci. Eng. C 107 (2020) 110219, https://doi.org/10.1016/j.msec.2019.110219.